Chapter 11
The One-Dimensional-Turbulence Model

Tarek Echekki, Alan R. Kerstein, and James C. Sutherland

Abstract The one-dimensional turbulence (ODT) model represents an efficient and novel multiscale approach to couple the processes of reaction, diffusion and turbulent transport. The principal ingredients of the model include a coupled deterministic solution for reaction and molecular transport and a stochastic prescription for turbulent transport. The model may be implemented as stand-alone for simple turbulent flows and admits various forms for the description of spatially developing and temporally developing flows. It also may be implemented within the context of a coupled multiscale solution using the ODTLES approach. This chapter outlines the model formulation, and applications of ODT using stand-alone solutions and ODTLES.

11.1 Motivation

In his survey of turbulent combustion modeling, Norbert Peters [25] emphasizes the difficulties that can arise due to the interactions between turbulence and chemistry over a wide range of length and time scales. Assumptions about inertial-range scaling of the turbulent cascade are not necessarily applicable, and there are few if any formal or conceptual constructs to which the modeler can turn when these scalings do not apply. He notes important empirical evidence that gross features of turbulent combustion often conform to inertial-range phenomenology, particularly with regard to its most important consequence for combustion: the length and time scale

Tarek Echekki
North Carolina State University, Raleigh, NC, USA, e-mail: techekk@ncsu.edu

Alan R. Kerstein
Sandia National Laboratories, Livermore, CA, USA, e-mail: arkerst@sandia.gov

James C. Sutherland
The University of Utah, Salt Lake City, UT, USA, e-mail: James.Sutherland@utah.edu

T. Echekki, E. Mastorakos (eds.), *Turbulent Combustion Modeling*,
Fluid Mechanics and Its Applications 95, DOI 10.1007/978-94-007-0412-1_11,

separation between the dominant large-scale turbulent motions and the small scales of molecular transport and chemical kinetics in flames. Many existing models rely on this scale separation, while the linear-eddy model (LEM: see Chapter 10) and one-dimensional turbulence (ODT) do not. To the extent that scale separation is not obeyed in turbulent combustion processes, LEM and ODT can be especially suitable for modeling these processes.

Peters discusses the role of scale invariance as well as scale separation in the inertial range. The latter is more general: scale separation is possible in the absence of scale invariance, but there is no scale invariance without scale separation (see below). Scale invariance of spectral energy transfer in turbulence, in conjunction with (and in fact, relying on) the negligible influence of viscous dissipation in the inertial range (an idealization, but valid in this context), imply that the characteristic eddy time scale $\tau(l)$ at length scale l obeys the dependence $\tau(l) \sim l^{2/3}$. This implies power-law dependences of eddy velocity, energy, and diffusivity, and ultimately, scale separation between inertial-range and dissipation-range processes.

LEM resolves all advective, diffusive, and chemical length and time scales of turbulent combustion, and hence does not rely on scale separation. It represents thermal expansion by means of dilatation of the 1D domain, but it does not model other aspects of feedback from combustion to turbulent motions, such as viscosity variations and turbulence generation by expansion. In particular, the probability distribution function (pdf) from which the maps representing turbulent eddies are sampled has a fixed functional form whose construction is guided by the inertial-range diffusivity scaling (Chapter 10). To the extent that turbulence-chemistry interactions result in deviations from this scaling, the fidelity of LEM can be impaired. Other influences, such as rapid transients caused by initial conditions or time-varying boundary conditions, can also cause significant deviations from inertial-range scalings.

As noted, there is little theoretical guidance on how to model the deviations from inertial-range scalings that might be caused by these influences or the effects of these deviations on combustion dynamics. Within the 1D stochastic approach based on the triplet-map representation of turbulent eddies (see Chapter 10), incorporation of these influences is therefore approached from an entirely different perspective.

This perspective is introduced by first considering direct numerical simulation (DNS) of turbulent combustion. In DNS, no theory or guiding principle is needed to capture combustion-induced deviations from inertial-range scaling because the underlying equations of motion are solved. Thus, the consequences of turbulence-chemistry interactions are outcomes of the simulated flow evolution that do not require prior analysis or modeling. To the extent that the local, time-resolved interactions between turbulent eddy motions and combustion processes can be represented robustly with the 1D stochastic framework, that framework can likewise capture their consequences as outcomes of simulated evolution.

A formulation with this capability becomes, in effect, a broadly predictive model of turbulent flow evolution rather than a model focused, as LEM is focused, on simulation of mixing and reaction in a parametrically specified turbulent environment. Thus, the quest for a robust turbulent combustion model leads ultimately to reconsideration of turbulence modeling more generally. This is the context in which ODT

was originally formulated. The stages of its development for application to free and confined shear flows, variable-density flows, buoyant stratified flows, and multiphase flows, as well as combustion and other reacting flows, have been documented in references cited below.

To introduce ODT, a formulation applicable to constant-property flow is outlined. Algorithmic as well as physical modeling considerations are discussed. Extensions needed for combustion applications and representative examples are described. Use of ODT for subgrid modeling in 3D simulations of constant-property flow and of combustion is discussed, and future prospects are assessed.

11.2 Constant-Property ODT

11.2.1 Model Formulation

ODT is introduced with reference to LEM by formulating LEM in a notation that carries over directly to ODT. An eddy rate distribution $\lambda(y_0,l;t)$ is defined by setting $\lambda(y_0,l;t)\,dy\,dl$ equal to the expected number, per unit time, of eddies for which the lower boundary of the eddy is in $[y_0,y_0+dy]$ and the eddy size is in the range $[l,l+dl]$. In terms of Λ and $f(l)$ defined in Chapter 10, $\lambda(y_0,l;t)=\Lambda f(l)$. Thus, the units of λ are 1/(length$^2\times$time) and its integral over eddy sizes l is Λ.

In LEM, λ has no dependence on y_0 or t unless one chooses to hard-wire such dependence into Λ or $f(l)$, which has been done in some instances, e.g., [13]. ODT is formulated to incorporate such dependence in a way that reflects the relationship between the likelihood of an eddy, quantified by the eddy time scale τ, and the local flow state. This requires the introduction of a local, instantaneous representation of the flow state in ODT, causing ODT to be a fundamentally different type of model than LEM, whose turbulent state is characterized parametrically.

The flow representation in ODT consists of 1D profiles of one or more velocity components whose evolution, in the simplest constant-property formulation, is qualitatively the same as in LEM applied to a constant-density passive scalar. For example, with one velocity component $u(y,t)$, time advancement is governed by

$$\frac{\partial u}{\partial t}=\nu\frac{\partial^2 u}{\partial y^2}, \tag{11.1}$$

where ν is the kinematic viscosity. This advancement is punctuated by 'eddy events,' each of which consists of a triplet map (defined and explained in Chapter 10) applied to the u profile, possibly (depending on the formulation) followed by another operation that is described shortly. Absent the latter, the evolution of u is equivalent to the evolution of a constant-property passive scalar in LEM, except for the crucial distinction that $\lambda(y_0,l;t)$ is now a specified function of the current flow state $u(y,t)$. Several formulations of this dependence have been introduced during the course of ODT development. The formulation discussed here,

$$\lambda = \frac{C\nu}{l^4}\sqrt{\left(\frac{u_K l}{\nu}\right)^2 - Z}, \tag{11.2}$$

is a specialization of the formulation described in [17], which has a more detailed explanation of the motivation and features of ODT than can be provided here.

In Eq. 11.2, C and Z are free parameters whose roles are explained shortly, and for any property profile $s(y,t)$,

$$s_K \equiv \frac{1}{l^2}\int s(M(y))K(y)\,dy \tag{11.3}$$

defines s_K. Here, $M(y)$ is defined by the formal mathematical representation of the triplet map,

$$s(y) \rightarrow s(M(y)), \tag{11.4}$$

which indicates that the value of property s at $M(y)$ is mapped to location y. Thus, M is the operational inverse of the triplet map, which is formally convenient because M is a single-valued map but the triplet map is triple-valued. The 'kernel' $K(y) \equiv y - M(y)$ is the map-induced displacement of the point that is mapped to y by the triplet map. $K(y)$ thus depends on map parameters y_0 and l, but this dependence is suppressed in the condensed notation used here.

To explain the role of the kernel, the more general form of the eddy event in ODT is introduced. Namely, Eq. 11.4 is generalized to

$$s(y) \rightarrow s(M(y)) + c_s K(y), \tag{11.5}$$

which indicates that the eddy event applies the triplet map to property s and then adds the kernel times a coefficient c_s to $s(y)$. The kernel addition is applied only to velocity components and is intended to add or substract kinetic energy without changing the total momentum, which is assured for constant-density flow because $K(y)$ integrates to zero. This provides a mechanism for energy redistribution among velocity components when the formulation contains more than one component, enabling the model to simulate the tendency of turbulent eddies to drive the flow toward isotropy. Total energy must be conserved, imposing a constraint on the values of the coefficients c_s. The additional constraints needed to uniquely determine all the coefficients are obtained by requiring the kernel addition to produce an energy distribution within the eddy interval $[y_0, y_0 + l]$ that is as close to isotropic as possible. There are other reasonable criteria for determining the coefficients that might be advantageous in some cases [19]. In applications such as buoyant stratified flows or turbulent advection of immiscible liquids, eddy events might induce changes of the gravitational or surface-tension potential energy, requiring equal-and-opposite changes of kinetic energy. Through the kernel operation, conservation of total energy in ODT couples flow evolution to dynamically active scalars such as density in buoyant flows, as demonstrated in ODT studies of these flows [5, 15–17, 20, 35, 36, 38–40].

By construction, Eq. 11.5 conserves momentum for constant-density flow. For variable-density flow, a more general treatment is needed. Momentum conservation is no longer automatic, so extra degrees of freedom are introduced to enforce momentum conservation, further generalizing the eddy event as follows:

$$s(y) \rightarrow s(M(y)) + b_s J(y) + c_s K(y), \tag{11.6}$$

where $J(y) \equiv |K(y)|$ and the additional coefficients b_s are determined by requiring the eddy event to conserve the y-integrated momentum of all velocity components s. For details, see [1].

Most combustion applications of ODT pre-date this variable-density formulation, and several pre-date the introduction of the kernel formalism in Eqs. 11.2 and 11.5, so they do not include the kinetic-energy and variable-density phenomenology that can now be incorporated into ODT. The less complete treatment is adequate for many combustion applications, much as LEM, which is considerably simpler, is broadly useful for turbulent combustion simulation. The variable-density formulation is not discussed further here, but its future use, where appropriate, in ODT simulations of turbulent combustion is encouraged.

Before proceeding further, the guiding principle that motivates the model constructs introduced thus far is explained. Empirical evidence and formal analysis support the viewpoint that the turbulent cascade tends to be local in scale space, meaning that individual eddy motions such as vortex stretching typically shrink flow features in turbulence by order-one geometrical increments, such that the wide range of flow scales in turbulence is the cumulative outcome of many incremental scale reductions rather than a smaller number more drastic reductions.

Enforcement of this scale-locality principle in ODT is the basis of much of the model formalism. The triplet map decreases flow scales by no more than a factor of three. No other measure-preserving map induces less scale reduction. (Measure preservation assures that applicable conservation laws are obeyed.)

Energy changes during the eddy event are likewise consistent with scale locality. The kernel used for this purpose must be zero at the eddy endpoints (to prevent discontinuities) and must integrate to zero, so it must have at least two extrema. The function $K(y)$ consists of three linear segments over size-$l/3$ spatial intervals. Thus it introduces structure consistent with the scale reduction by the triplet map. The map is applied before the kernel because the kernel followed by the map would introduce structure at scale $l/9$.

Eddy selection as well as eddy implementation is guided by scale locality, in this case meaning that size-l motions are driven by size-l influences. Eddy phenomenology (i.e., mixing-length concepts applied to an individual eddy) suggests that λ should be of order $1/(l^2\tau)$, where τ is the eddy turnover time, or equivalently, $V(l)/l^3$, where $V(l)$ is the velocity difference between the eddy endpoints. The latter estimate, with numerical coefficients absorbed in the free parameter C of Eq. 11.2, was used in the original ODT formulation [15] and many subsequent applications. When kernels were introduced, the estimate $V(l) \sim u_K$ was adopted, which connects eddy selection to energy-based eddy implementation using an ex-

pression that measures velocity variations over an order-l distance, and hence is consistent with scale locality. In Eq. 11.2, the expression for λ involves a square root that contains a term proportional to u_K^2, hence a kinetic-energy term. In formulations involving multiple velocity components or other energy contributions such as gravitational potential energy, these contributions are additive under the square root.

A specific connection between u_K and eddy energetics is identified through consideration of the possible range of kernel-induced energy changes. Kernel addition can reduce the u kinetic energy within the eddy to zero only if the spatial profile of u within the eddy is proportional to the kernel function, so that kernel addition can make u identically zero within the eddy. Otherwise, there is a maximum amount of energy that can be extracted from the u profile by kernel addition that is less than the total u kinetic energy within the eddy. This maximum, termed the 'available energy' of the u component, is $(27/8)\rho l u_K^2$, where ρ is the density [19]. This connects u_K to flow energetics in various ways. For example, implementation of the isotropy criterion involves assignment of the coefficients c_s so as to equalize component available energies. In buoyant stratified flows, the available energy is the maximum kinetic energy that can be extracted in order to compensate for an equal-and-opposite change of gravitational potential energy. If there is less than the needed amount of available energy, then the eddy is energetically prohibited, so its λ value is set equal to zero.

The indication of a prohibited eddy is that the quantity in the square root in Eq. 11.2 is negative. The parameter Z is introduced so that an eddy can be prohibited even if there is net available energy. As indicated by the normalization of u_K in that equation, Z in effect sets a threshold Reynolds number for eddy turnover. Nonzero Z is not always required for good model performance, but in some instances it improves the results sufficiently to justify the introduction of an additional adjustable parameter. In some instances, Z is assigned a small positive value solely for computational efficiency. It prevents the implementation of unphysically small eddies that, if implemented, would have no noticeable effect on results of interest.

C is the main adjustable parameter of ODT. It scales the eddy event rate, and hence the simulated turbulence intensity, for a given flow configuration. In transient flows, it controls overall time development, e.g., the spreading rate of free shear flows.

Just as there can be a need to assign a positive Z value to suppress small eddies, there can be a need to suppress unphysically large eddies that would otherwise occur. This need arises primarily in simulations of free shear flows with laminar co-flows or free streams. Eddies much larger than the width of the turbulent region can have enough available energy to enable their occurrence. (For a planar mixing layer, the difference between the free-stream velocities can provide enough available energy irrespective of any turbulence.) Such eddies violate the scale-locality requirement that the scale of the flow features that provide the available energy for eddy occurrence should be of the order of the eddy size.

Several large-eddy-suppression procedures have proven useful. One that is found to work particularly well for jets and jet diffusion flames [7, 27] requires that τ (which is l/u_K in the formulation described here) must be less than the elapsed flow-

advancement time times an adjustable coefficient, otherwise the eddy is prohibited. The introduction of an additional free parameter is found to be well justified by the resulting model performance. An alternative that was used to simulate mixing layers [1] and buoyant fire plumes [31] is the scale-reduction method, in which the eddy is divided into three equal parts and each of these must be found to have enough available energy for eddy turnover (based on a small Z value that negates any numerical noise contribution; results are insensitive to the chosen value), otherwise the eddy is prohibited. If not prohibited based on this test, the eddy is processed in the usual manner.

11.2.2 Numerical Implementation

Based on Eq. 11.3, u_K and thus λ depend on y_0 and l, and this dependence is time varying due to the time advancement of $u(y,t)$. Therefore at each instant there is a new eddy rate distribution from which individual eddy events are to be sampled. Computation of, and sampling from, this two-parameter distribution on an ongoing basis is computationally unaffordable. Therefore, the thinning algorithm [22] for efficient sampling from nonstationary Poisson processes (which is a generalization of the von Neumann rejection method) is employed. A fixed eddy rate distribution $\hat{\lambda}$ is constructed so as to oversample all eddies, i.e., it exceeds the true λ value for all y_0, l, and t. When an eddy is sampled from the fixed distribution, the true λ value for that eddy based on the flow state at that instant is computed and the eddy is accepted with probability $\lambda/\hat{\lambda}$, otherwise rejected. This approach strongly influences many aspects of algorithm formulation and coding.

ODT has been implemented numerically using both uniform and adaptive meshes. On a uniform mesh, the triplet map is implemented as a permutation of mesh cells. On an adaptive mesh, the mathematical definition of the triplet map on the spatial continuum is applied. Properties are assumed constant within each cell, so the continuum triplet map is applied to piecewise constant continuum property profiles. This involves mapping cell faces, which creates new faces because the map is multi-valued, and assigning cell property values accordingly.

The uniform-mesh implementation is described in many of the publications that have been cited, and a uniform-mesh code and documentation are available for download [9]. The adaptive-mesh implementation is explained and applied in [31].

11.2.3 Generalizations and Couplings

The adaptive mesh facilitates several generalizations of ODT that are difficult to implement on a uniform mesh. It allows Lagrangian rather than Eulerian implementation of advection (in the conventional sense), which is useful for incorporating thermal expansion and for implementing spatial (streamwise) rather than temporal

advancement of ODT. Spatial advancement conserves property fluxes rather than properties. Flux conservation requires an implementation of continuity that involves dilatations along the 1D domain, which are convenient to implement in a Lagrangian manner. The numerics of Eulerian spatial advancement are especially challenging for variable-property flows. This motivated the introduction of an adaptive mesh to simulate the vertical spatial development of a fire plume [31]. Variable-property spatial advancement has been implemented on a uniform mesh by performing a Lagrangian sub-step and then interpolating the displaced mesh back to the fixed uniform mesh [1].

The adaptive mesh also facilitates ODT implementation in cylindrical geometry, in which triplet maps must conserve $r\,dr$ rather than dy. In this case, the triplet map is not readily approximated by permuting the cells of a uniform mesh. An adaptive-mesh implementation of a cylindrical spatial formulation has been used to simulate round jet diffusion flames [21]. An earlier cylindrical LEM formulation on a uniform mesh [14] conserves ensemble averages but is not locally conservative, which is less desirable but adequate for some purposes.

A spatially advancing ODT realization can be interpreted as a 2D flow snapshot. On this basis, a spatially advancing fire-plume simulation [31] has been used to compute 2D radiation fields, which are then used to specify the background radiation field for the next simulated realization. This alternation between ODT and the radiation computation was iterated to statistical convergence to obtain a coupled flow-radiation solution.

Another physical process that has been coupled to the ODT flow simulation is inertial-particle response to turbulent motions (one-way coupling). This formulation has been used to simulate wall deposition in channel flow [34].

For some applications, full spatial resolution is unaffordable even in 1D. Therefore various approaches to subgrid closure in ODT have been developed and applied [20, 24].

Chapter 10 describes ways in which LEM domains have been coupled to under-resolved 3D flow simulations to provide mixing and chemistry closure. ODT has the capability to provide subgrid momentum closure as well, as demonstrated in applications to channel flow [33] and homogeneous decaying turbulence [32]. Various formulations of ODT-based 3D flow simulation have been proposed [17, 18, 23]. Formulations that have been used for combustion simulation are described in Sect. 11.3.3.

11.2.4 Features of the ODT Representation of Turbulent Flow

The ODT representation of a time-developing Kelvin–Helmholtz instability, illustrated in Fig. 11.1, indicates some of the flow features captured by the model. This illustration is based on the ODT formulation of [19].

The rendering shows that the width of the active mixing zone grows primarily by the relatively infrequent occurrence of a large event extending beyond the current

range of the mixing zone, with some additional contribution by the more numerous small events. This process is consistent with the dominant role of large engulfing motions and the secondary role of small-scale nibbling in turbulent entraining flows under neutral-buoyancy conditions. (The effect of density stratification on the ODT representation of turbulent entrainment has been investigated [1, 15].)

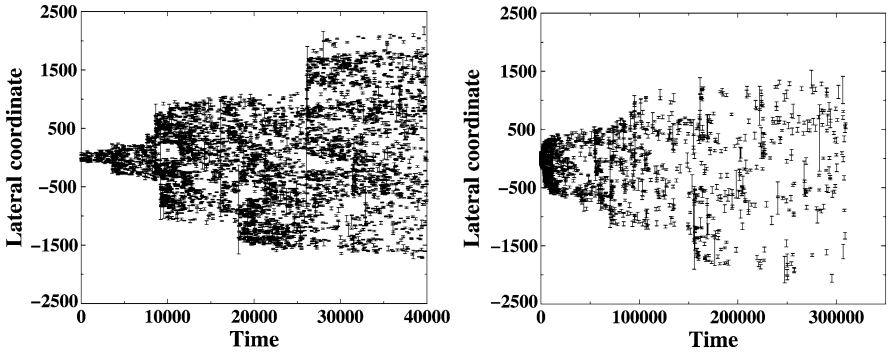

Fig. 11.1: Graphical representation of the sequence of eddy events during a simulated ODT realization of a time-developing Kelvin–Helmholtz instability (left panel) and a time-developing planar wake (right panel) [19]. The Kelvin–Helmholtz and wake simulations are initialized using step-function and top-hat initial velocity profiles, respectively. The space and time units in this illustration are arbitrary. In the plots, each eddy is represented by an error bar whose vertical span corresponds to the eddy range $[y_0, y_0 + l]$, and whose horizontal location corresponds to the time of eddy occurrence. Reprinted from [19] with permission. Copyright © 2001, Cambridge University Press.

Bunching of events, especially after the occurrence of a large event, reflects the interactions between the eddy events and the evolving velocity profile that induce the model analog of the turbulent cascade. Each eddy event compresses and folds the velocity profile within the range of the eddy. This increases the local shear and thus the available energy that determines the frequency of subsequent eddies within that range. A feedback process is thus induced that promotes the occurrence of successively smaller eddies. Eventually, velocity fluctuation length scales are reduced sufficiently so that damping of the fluctuations by concurrent viscous transport dominates the production of fluctuations by eddies. Viscous damping thus terminates the local burst of eddy activity.

A planar-wake simulation is also shown in Fig. 11.1. In the Kelvin–Helmholtz simulation, vigorous turbulence, indicated by the number and size range of eddies as the flow evolves, is sustained by the shear imposed on the flow by the free-stream conditions (far-field velocity difference). The wake, however, evolves in a uniform background. As the initial velocity perturbation is dispersed by eddies and dissi-

pated by concurrent viscous evolution, the turbulence intensity decreases, affecting the eddy frequency and size range and slowing the growth of the turbulent zone. These qualitative impressions are supported by the quantitative consistency of ODT simulation statistics with the known similarity scalings for these flows [19].

11.3 Applications of ODT in Combustion

Like its predecessor, LEM (see Chapter 10), the ODT model may be implemented either as a stand-alone model or within the context of a 3D solution, such as LES. The stand-alone ODT model may also serve a similar role to direct numerical simulations (DNS) for the construction of libraries for turbulence-chemistry interactions [28–30]. ODT stand-alone models are limited in scope to flows with one dominant flow direction, where a boundary-layer like solution may be adopted. Similar to LEM, the implementation of ODT within the context of more complex flows may be achieved through the coupling of ODT with a coarse-grained simulation approach, such as LES [3].

There are many variants of the ODT model in the literature. The modeling approach is typically explained by combining the discretization, solution algorithm, and governing equations. In Sect. 11.3.1, we present a unified method by which all of the approaches in the literature may be derived, along with a brief discussion of the equations ultimately used by in the various approaches.

Section 11.3.2 then presents a sampling of results from stand-alone ODT simulations of turbulent combustion.

11.3.1 Governing Equations

This section presents a brief discussion of the various forms of the governing equations presently solved in ODT. A more detailed exposition can be found in [37].

A generic balance equation for an intensive property ψ in a control volume (CV) V enclosed by surface S can be written as

$$\int_{\mathsf{V}(t)} \frac{\partial \rho \psi}{\partial t} \mathrm{d}\mathsf{V} + \int_{\mathsf{S}(t)} \rho \psi \left(\mathbf{v}_r + \mathbf{v}_s\right) \cdot \mathbf{a} \mathrm{d}\mathsf{S} = - \int_{\mathsf{S}(t)} \boldsymbol{\Phi}_\psi \cdot \mathbf{a} \mathrm{d}\mathsf{S} + \int_{\mathsf{V}(t)} \sigma_\psi \mathrm{d}\mathsf{V}, \quad (11.7)$$

where $\mathbf{v}_s$ is the velocity of the surface S, $\mathbf{v}$ is the mass-averaged velocity, $\mathbf{v}_r = \mathbf{v} - \mathbf{v}_s$ is the velocity of the fluid relative to the surface, ρ is the density, $\boldsymbol{\Phi}_\psi$ is the mass diffusive flux of ψ, and σ_ψ is the volumetric rate of production of ψ. Table 11.1 defines the terms ψ, $\boldsymbol{\Phi}_\psi$, and σ_ψ for various quantities. These equations are closed with an appropriate equation of state relating the local pressure to the composition, density and temperature.

Table 11.1: Definition of terms in (11.7) for some common governing equations. Here $\boldsymbol{\tau}$ is the stress tensor, $\mathbf{g}$ is the gravitational acceleration vector, Y_k is the mass fraction of species k, $\mathbf{j}_k$ is the species diffusive flux vector, and $\mathbf{q}$ is the heat flux vector. Other equations may be added as necessary. This is just a partial representation of commonly solved equations.

Equation	ψ	Non-convective Flux, $\boldsymbol{\Phi}_\psi$	Source Term, σ_ψ
Continuity	1	0	0
Momentum	$\mathbf{v}$	$p\mathbf{I}-\boldsymbol{\tau}$	$\rho\mathbf{g}$
Species	Y_k	$\mathbf{j}_k$	σ_k
Total Internal Energy	e_0	$p\mathbf{v}+\boldsymbol{\tau}\cdot\mathbf{v}-\lambda\nabla T+\sum_{k=1}^{n}h_k\mathbf{j}_k$	$\rho\mathbf{g}\cdot\mathbf{v}$
Internal Energy	e	$\mathbf{q}$	$\boldsymbol{\tau}:\nabla\mathbf{u}-p\nabla\cdot\mathbf{u}$
Enthalpy	h	$\mathbf{q}$	$\frac{\partial p}{\partial t}+\mathbf{u}\cdot\nabla p+\boldsymbol{\tau}:\nabla\mathbf{u}$

In the following, we present the various forms of the governing equations in use for ODT. Much of the treatment of the governing equations for ODT in the literature combine the governing equations with the numerical algorithm. The following does not address numerical solution techniques for the equations; rather, we focus on a unified approach for arriving at the various forms of the governing equations implied by present ODT approaches in the literature.

11.3.1.1 Temporally Evolving Lagrangian Formulation

The first ODT formulations employed a temporally evolving formulation in a Lagrangian frame of reference. In this case, we have $\mathbf{v}=\mathbf{v}_s$ so that $\mathbf{v}_r=0$. Writing (11.7) in one dimension and using the continuity equation ($\psi=1$) to convert it to the weak form yields

$$\frac{\mathrm{d}\psi}{\mathrm{d}t}=\frac{1}{\rho}\left[-\frac{\partial\Phi_{\psi,y}}{\partial y}+\sigma_\psi\right]. \tag{11.8}$$

In (11.8), $\frac{\mathrm{d}\psi}{\mathrm{d}t}$ represents the local change of ψ as it moves at velocity v_s, $-\frac{1}{\rho}\frac{\partial\Phi_{\psi,y}}{\partial y}$ is the change in ψ due to diffusion, and $\frac{\sigma_\psi}{\rho}$ is the change in ψ due to consumption/production.

Implementations of this approach use moving meshes and finite-volume schemes. The CV surface positions can be determined by solving (11.8) for $\psi=v$ (the lateral fluid velocity) and an ODE for position,

$$\frac{\mathrm{d}y}{\mathrm{d}t}=v=v_s. \tag{11.9}$$

Rather than solving (11.8) for $\psi=v$, however, most ODT formulations employing the temporally evolving Lagrangian formulation instead use a discrete form of the

continuity equation written in Eulerian coordinates, $\frac{\partial \rho}{\partial t} = -\frac{\partial v_s}{\partial y}$ together with the assumption of constant pressure and an equation of state to solve for v_s for use in (11.9).

11.3.1.2 Temporally Evolving Eulerian Formulation

Recently, an Eulerian temporally evolving formulation for the ODT equations was proposed [26, 27]. In the Eulerian frame of reference, we fix the CV surface positions so that $\mathbf{v}_s = 0$ and $\mathbf{v}_r = \mathbf{v}$ so that (11.7) becomes, in differential form,

$$\frac{\partial \rho \psi}{\partial t} = -\nabla \cdot \rho \psi \mathbf{v} - \nabla \cdot \boldsymbol{\Phi}_\psi + \sigma_\psi. \tag{11.10}$$

The one-dimensional differential form of (11.10) is

$$\frac{\partial \rho \psi}{\partial t} = -\frac{\partial \rho \psi v}{\partial y} - \frac{\partial \Phi_{\psi,y}}{\partial y} + \sigma_\psi. \tag{11.11}$$

The velocity v in (11.11) represents the local fluid velocity in the y-direction, and $\frac{\partial \rho \psi}{\partial t}$ represents the local change in $\rho \psi$ at a given point in space and time. Current approaches using the Eulerian form have solved the compressible form of these equations [26, 27]. The equations solved are given by (11.10) and Table 11.1, where $\psi = 1$ is solved for ρ, $\psi = v$ and $\psi = u$ are solved for the lateral and streamwise momentum components, $\psi = e_0$ is solved for the total internal energy, $\psi = Y_k$ is solved for the species mass fractions, and an equation of state is used to relate T, p, ρ, and Y_k.

11.3.1.3 Space-Time Mapping

The equations discussed above (both the Lagrangian and Eulerian forms) provide solutions with (t, y) as independent variables. Frequently, however, we require solutions that evolve spatially (e.g., when comparing with data from a spatially evolving jet). This requires a space-time mapping, achieved by solving an ODE for streamwise position,

$$\frac{\mathrm{d}x}{\mathrm{d}t} = \bar{u}, \tag{11.12}$$

where $\bar{u}$ is a suitably chosen average velocity for advection of the ODT domain in the streamwise direction. This creates an approximate 'average' location of the line in space. Of course, the line would actually tend to bend due to variations in u. This is explicitly ignored by adopting an average velocity, $\bar{u}$, that advects the line downstream. One possible choice for $\bar{u}$ is

$$\bar{u}(t) = u_\infty + \frac{\int_{-\infty}^{\infty} \rho (u - u_\infty)^2 dy}{\int_{-\infty}^{\infty} \rho (u - u_\infty) dy}. \tag{11.13}$$

An alternative approach to using the approximate space-time mapping (11.12) is to reformulate the governing equations with (x,y) as independent variables rather than (t,y). This is considered in the following sections for both the Lagrangian and Eulerian frames of reference.

11.3.1.4 Spatially Evolving Lagrangian Formulation

The spatially evolving Lagrangian formulation is obtained from (11.7) by choosing $\mathbf{v}_s \cdot \mathbf{x} = 0$ and $\mathbf{v}_s \cdot \mathbf{y} = v$. Then assuming steady state, 2D, and writing the differential equation in weak form (using the continuity equation), (11.7) becomes

$$\frac{\mathrm{d}\psi}{\mathrm{d}x} = -\frac{1}{\rho u}\left[\frac{\partial \Phi_{\psi,y}}{\partial y} - \sigma_\psi\right]. \tag{11.14}$$

In deriving (11.14), we have neglected the streamwise diffusive term, $\frac{\partial \Phi_{\psi,x}}{\partial x}$. This term is neglected primarily for practical algorithmic reasons. However, in application to spatially evolving jets, diffusion in the lateral direction will likely dominate any diffusion in the downstream direction. Nevertheless, this is an assumption in the spatial ODT formulations.

This approach has been adopted by Ricks et al. [31] to perform spatially evolving simulations of buoyant pool fires including soot transport and radiation (see Sec. 11.3.2).

11.3.1.5 Spatially-Evolving Eulerian Formulation

The spatially evolving form of the equations for ODT in Eulerian form is obtained from (11.10) by assuming steady state and variation only in x and y. Then using the continuity equation to write it in weak form and neglecting $\frac{\partial \Phi_{\psi,x}}{\partial x}$ as we did in (11.14), we find

$$\frac{\partial \psi}{\partial x} = -\frac{1}{\rho u}\left[\rho v \frac{\partial \psi}{\partial y} + \frac{\partial \Phi_{\psi,y}}{\partial y} - \sigma_\psi\right]. \tag{11.15}$$

11.3.2 Stand-Alone ODT Simulations

As a stand-alone model, ODT has been implemented for the study of jet diffusion flames [7, 11, 12, 21, 27–30], buoyant fire plumes [31], flame spread [35], and autoignition in jet flows [6]. In these studies different model formulations have been implemented, which illustrate the versatility of the ODT modeling framework. We start with the temporally-evolving Lagrangian formulation, which has been adopted for high-Reynolds number jets, but may be implemented as well for compressible

turbulent shear layers and wall-bounded flows. We then illustrate the temporally evolving Eulerian formulation for temporally evolving shear layers [27] and the temporally evolving Lagrangian formulation for buoyant fire plumes [31]. In all formulations, a deterministic solution, involving diffusion, reaction and advective transport operators in the Eulerian formulation, in conjunction with a stochastic implementation of turbulent advection, is implemented.

The temporally evolving Lagrangian formulation is based on the solution of equation (11.8) for the streamwise (x) component of momentum along with equations for energy and species. Figure 11.2 shows temperature contours for a wall fire from [35] from a single (left) and 300 (right) realizations. This was solved using the temporal formulation with (11.12) to provide an approximate space-time mapping. Close examination reveals that small scale triplet mapping events are first observed at approximate heights of 25 cm and at a distance of approximately 2 cm away from the wall corresponding to the high values of temperature (and velocity, not shown). As the flow further accelerates, progressively larger eddy stirring events are shown to occur causing larger scale macro-mixing and the engulfment of the surrounding air. This transition of energy from small to large scales of motion is also consistent with recent observations from experiments and LES predictions of large scale plumes [4].

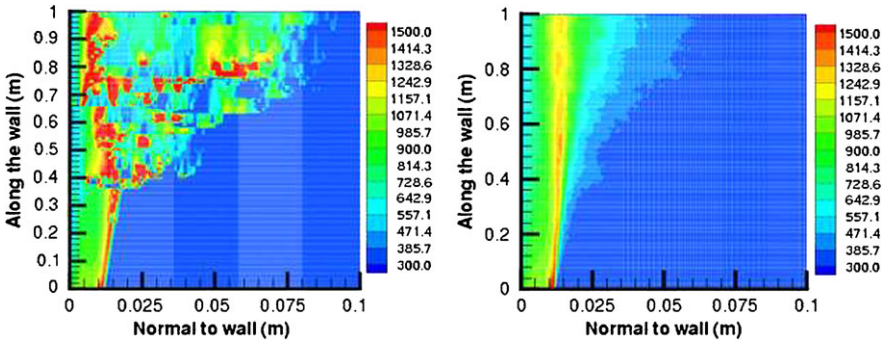

Fig. 11.2: 2D renderings of temperature corresponding to a single realization (left) and averaged (right) over 300 realizations of a wall fire. From [35].

Results from a piloted jet flame simulation with extinction and reignition are shown in Figure 11.3 for the same formulation. The results illustrate how the ODT model is able to predict extinction and reignition in piloted turbulent non-premixed flames. Two zones may be identified in the jet flame. The first corresponds to a region extending approximately fifteen diameters downstream from the inlet that illustrates a transition from piloted burning to extinction. This transition is followed by a gradual reignition as shown by the increased OH mass fraction. The 2D rendering of stirring events also shows that stirring events are initiated at the interfaces

between the fuel jet and the pilot flow and the interfaces between the pilot flow and the co-flow air, and that the size of eddies progressively increases as a function of downstream distance, emulating the progressive growth of the shear layers. Evidence of the existence of an 'energy cascade' in the ODT solutions is demonstrated by the presence of smaller eddies that trail larger eddies, with regions of spatial intermittency, as these smaller eddies dissipate (see also Fig. 11.1).

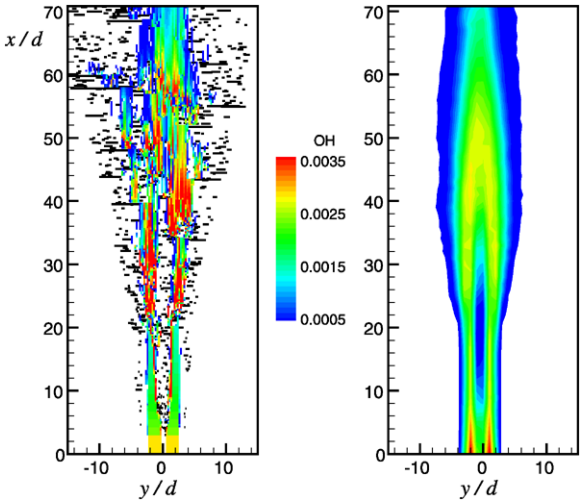

Fig. 11.3: 2D renderings of OH mass fraction corresponding to a single realization (left) and averaged (right) over 100 realizations of Sandia piloted methane-air flame F. The 1D domain corresponds to the horizontal axis. Its temporal evolution is converted to a downstream distance based on (11.12) and (11.13). Reprinted from [30] with permission from Taylor and Francis.

The formulation proposed by Punati et al. [26, 27] solves the Eulerian form of the governing equations described in Sec. 11.3.1. Specifically, (11.10) is solved with $\psi = \left(\rho \ \rho v \ \rho u \ \rho e_0 \ \rho Y_i\right)$, where u is the streamwise velocity and v is the velocity component in the direction of the the ODT line orientation. See Table 11.1 for definitions of the diffusive fluxes in these equations. These equations are solved together with the ideal gas equation of state, detailed CO/H_2 oxidation kinetics, and mixture-averaged transport to make direct comparison with DNS data of a planar, temporally evolving CO/H_2-air nonpremixed jet [10]. The DNS dataset includes extinction and reignition, with the onset of extinction at a characteristic jet time of $\tau \approx 20$ and reignition occurring at around $\tau \approx 30$. This calculation allowed direct comparison between the ODT and DNS data. Initial conditions were extracted directly from the DNS data, and all treatment of diffusion, thermodynamics, and chemical kinetics was equivalent.

Figure 11.4 shows the average and RMS velocity and mixture fraction profiles for the ODT and DNS simulations. The spreading rate is well captured by ODT. The RMS profiles are captured reasonably, but the ODT under-represents the magnitude of the RMS fluctuations. Similar trends hold for all species (including minor species), with the exception that extinction is over-predicted by the ODT simulations.

Figure 11.5 shows the evolution of the probability density functions conditioned on lean and rich mixture fractions for the temperature and scalar dissipation rate. The temperature PDF illustrates that the ODT predicts an earlier onset of extinction than the DNS. Specifically, at $\tau = 6$ there is already evidence of extinction in the ODT data. However, the extinction-reignition process is captured relatively well despite these differences.

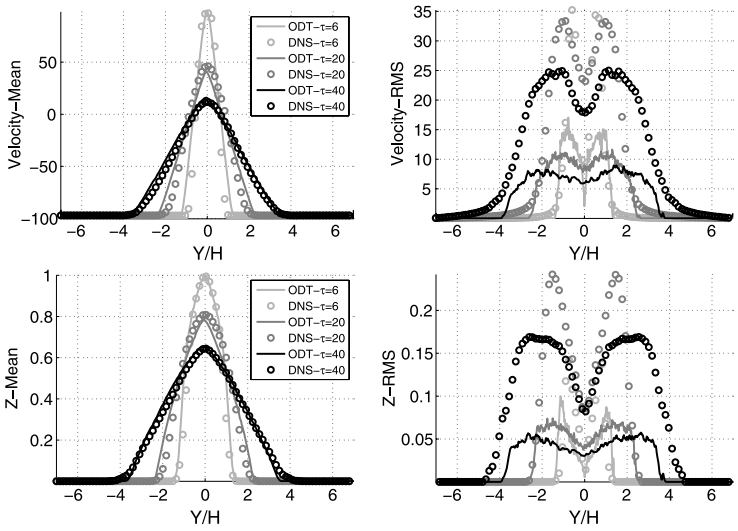

Fig. 11.4: Evolution of the streamwise velocity (top) and mixture fraction (bottom) showing the mean (left) and RMS (right) for the ODT (lines) and DNS (circles) data. Results are shown for characteristic jet times from $\tau = 6$ to $\tau = 40$. From [27].

The data shown in Figs. 11.4 and 11.5 were obtained from 400 ODT realizations, and each realization required approximately two CPU hours. In contrast, the DNS calculations (which were three-dimensional) required several million CPU hours. Although ODT cannot capture uniquely multidimensional effects that DNS can, it does represent many of the physical processes present in true three-dimensional turbulent flow at a fraction of the cost of DNS, and thus serves as a very useful tool in combustion modeling.

Ricks et al. [31] simulated a buoyant fire plume using ODT by solving (11.14) (the spatially evolving form of the governing equations in Lagrangian form) as outlined in Sect. 11.3.1, including transport equations for solid-phase soot particles as

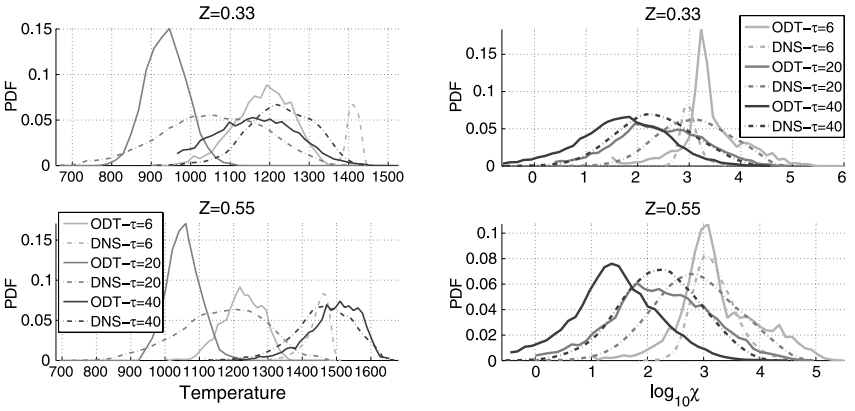

Fig. 11.5: Conditional pdf of temperature (left) and scalar dissipation rate (right). Results are shown for lean and rich mixture fractions and three different times during the jet evolution. DNS data is shown dot-dash lines and ODT data is shown with solid lines. From [27].

well as gas-phase transport equations. However, Ricks et al. [31] adopt a simplified approach for the representation of the gas phase species using the flamelet assumption and transporting the gas phase mixture fraction. In this formulation, the two independent variables correspond to the lateral (along the ODT domain) coordinate, y, and the streamwise spatial coordinate, x. The 1D nature of the solution enables the implementation of a host of models for soot evolution (including soot oxidation by OH), and transport (including thermal diffusion), radiation and gas phase chemistry on large-scale computational domains.

Figure 11.6 shows 2D renderings of the temperature corresponding to two separate realizations of the ODT simulation of a fire plume by Ricks et al. [31]. The ODT domain is aligned with the horizontal direction (x); a marching algorithm is implemented to evolve the ODT solution in the vertical (y) direction on a computational domain of 2 m $\times$ 3 m. The necking just above the base of the flame is due to the spatial form of the continuity enforcement, which induces inward lateral flow in order to compensate for the buoyancy-induced increase in the streamwise mass flux. Additional statistics on soot evolution and radiation effects may be found in [31].

11.3.3 Hybrid ODTLES

Similarly to LEM, ODT may be coupled to a 3D coarse-grained simulation approach, such as LES, for chemistry and mixing closure. Moreover, there are different strategies for LES and ODT coupling based on Eulerian and Lagrangian for-

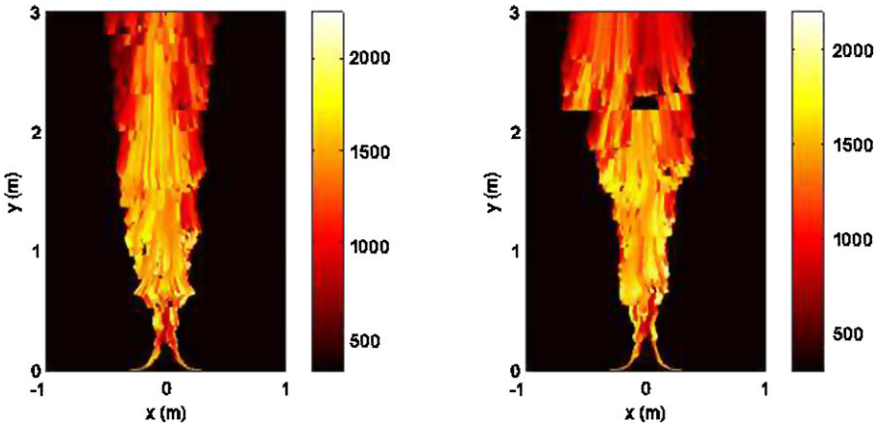

Fig. 11.6: 2D renderings of temperature (in K) corresponding to two separate realizations of a buoyant fire plume simulation. Reprinted from [31] with permission from Taylor and Francis.

mulations. In both formulations, ODT domains or elements are embedded in 3D solutions to resolve subfilter-scale momentum and scalar statistics. In the Eulerian formulation, ODT elements are fixed in space. Advective transport contributions in this formulation are represented by both large-scale transport resolved by LES and subfilter-scale transport represented by ODT stirring events. The simplest Lagrangian formulation may be implemented by attaching ODT solutions along the normal to the flame brush. In this formulation, the ODT elements are advected along with this brush. Similar strategies have been successfully adopted with LEM as discussed in Chapter 10.

In contrast to LEM, the coupling of LES with ODT may present a number of additional advantages:

- ODT has the capability to provide closure for momentum. However, one may choose to provide closure for scalars only and allow for a standard model for momentum closure (as discussed below).
- In ODT, the coupling of momentum and scalars is implemented on the fine time and length scales of ODT solutions; this coupling is very crucial near physical boundaries (e.g. walls) where both scalar and momentum boundary conditions may be implemented.
- Historically, large-scale transport with LES-LEM has been implemented using 'splicing' events, which extract segments from a LEM solution in one LES grid and transfers them to another LEM solution in a neighboring LES cell. The LES-ODT formulation of Cao and Echekki [3] proposes an alternative representation for large-scale transport based on ODT domains extending beyond a single LES cell.

The ODTLES model formulation is illustrated using the Eulerian formulation by Cao and Echekki [3]. The ODTLES formulation is based on two simulations that are implemented in the same computational domain. The first is a 3D LES for mass and momentum transport. The second is based on fine-grained simulations implemented on an ensemble of 1D ODT elements, which are embedded in the LES domain. Here, we describe a formulation in which ODT elements are distributed in a 3D Cartesian lattice as shown in Fig. 11.7 where the LES is solved on a structured Cartesian grid as well. However, a more complex layout may be adopted. Moreover, the formulation is used primarily for reactive scalars closure. For momentum closure, a 'standard' LES closure model for subgrid stresses may be adopted.

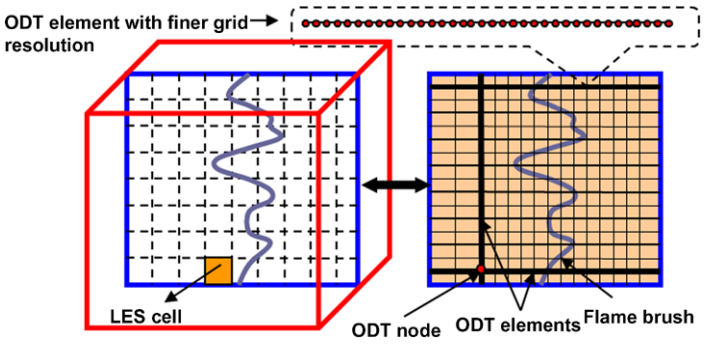

Fig. 11.7: Layout of ODT elements on a Cartesian grid in LES. Adapted from [3].

The ODT governing equations are solved on each individual ODT element. The temporal and spatial resolution requirements in ODT are similar to those needed for direct numerical simulations. The coordinate system on which the governing equations are based is a Cartesian coordinate system with one component along the ODT domain, x_1, and two additional orthogonal components, x_2 and x_3. The spatial coordinate, x_1, replaces the ODT domain coordinate, y, in previous discussions. When laid out on a Cartesian lattice, the direction x_1 represents the axis that is aligned with the ODT element; while the other coordinates x_2 and x_3 represent the remaining axes. The velocity field is split into a filtered (resolved in LES) component and a residual component:

$$u_i = \tilde{u}_i + u_i^* \tag{11.16}$$

where $\tilde{u}_i$ is the filtered velocity in the ith direction. The contribution of transport due to this velocity component is denoted as large-scale transport. The second term on the right-hand side, u_i^*, is the residual term of the velocity field in the ith direction. This latter term is modeled using the stochastic turbulent stirring events in ODT. The contribution of transport due to this velocity component is denoted as subfilter-scale transport. The variable-density governing equations on each ODT element of momentum, temperature, and species mass fractions are:

- Momentum

$$\frac{\partial u_i}{\partial t} = + \left[\frac{1}{\rho} \frac{\partial \tau_{i1}}{\partial x_1} \right] + \left\{ - \frac{1}{\rho} \frac{\partial p}{\partial x_i} - \tilde{u}_j \frac{\partial u_i}{\partial x_j} + \frac{1}{\rho} \left(\frac{\partial \tau_{i2}}{\partial x_2} + \frac{\partial \tau_{i3}}{\partial x_3} \right) \right\} \tag{11.17}$$

- Temperature

$$\frac{\partial T}{\partial t} = \left[- \frac{1}{\rho c_p} \left(\frac{\partial q_1}{\partial x_1} + \sum_{k=1}^{N} h_k \omega_k \right) \right] - \left\{ \tilde{u}_j \frac{\partial T}{\partial x_j} + \frac{1}{\rho c_p} \left(\frac{\partial q_2}{\partial x_2} + \frac{\partial q_3}{\partial x_3} \right) \right\} \tag{11.18}$$

- Species $(k = 1, \ldots, N)$

$$\frac{\partial Y_k}{\partial t} = \left[\frac{1}{\rho} \left(- \frac{\partial j_{k1}}{\partial x_1} + \omega_k \right) \right] - \left\{ \tilde{u}_j \frac{\partial Y_k}{\partial x_j} + \frac{1}{\rho} \left(\frac{\partial j_{k2}}{\partial x_2} + \frac{\partial j_{k3}}{\partial x_3} \right) \right\} \tag{11.19}$$

In equations (11.17)-(11.19), the index j represents the sum over all three directions of the advective terms. The diffusive fluxes, j_{k1}, j_{k2} and j_{k3} correspond to mass diffusion fluxes of the k species in the x_1, x_2 and x_3 directions, respectively. They may be expressed as ρV_{k1}, ρV_{k2} and ρV_{k3}, where V_{ki} is the mass diffusion velocity of species k in the ith direction. q_1, q_2, and q_3 correspond to the components of the heat flux vector in the x_1, x_2 and x_3 directions, respectively. These components represent the contributions of heat conduction, heat transport by mass diffusion, the Dufour effect and radiative heat transport. The ODT governing equations feature contributions which are resolved on the ODT domain (terms inside brackets '[ ]'). These are the same source and transport terms present in the stand-alone ODT equations. The resolved contributions include (1) molecular transport with gradients along the 1D elements, (2) chemical and heat source terms, and (3) the subfilter-scale momentum and scalar transport; this latter term is represented by the ODT stochastic stirring events discussed in Sect. 11.2.1 and implemented on a range of length scales. Other contributions require gradients along the normal components to the ODT domain (terms inside brackets '{}'). The unresolved contributions include: (1) large-scale transport (advective transport based on the filtered velocity components), (2) molecular diffusion with gradients along x_2 and x_3, and (3) the pressure gradient terms in the momentum equations.

The coupling of LES and ODT solutions is implemented both temporally and spatially. The ODT integration treats reaction-diffusion, subfilter-scale transport (stirring events) and filtered-advection as parallel events that are integrated with their own time steps, and which are fractions of the LES time step. During the temporal integration of the two solutions, statistics are transmitted from one solution scheme to another. For ODT, the LES velocity field $\tilde{u}$ is evaluated from the LES solution of the momentum equations and interpolated onto the ODT elements' finer grids. For LES, a number of variables may be filtered from ODT solutions, including closure for the mass density, $\overline{\rho}$. In what follows strategies adopted for the integration of the various terms in the ODT equations are briefly discussed:

11.3.3.1 Molecular Processes

Molecular processes in the ODT governing equations include (1) reaction, (2) diffusion along the ODT elements' directions, and (3) diffusion along the directions normal to the ODT elements. The integration of the first two contributions is similar to their implementation in the stand-alone ODT formulation. The third contribution must be modeled. The treatment of the unresolved terms may be implemented either deterministically or stochastically. In the Cao and Echekki [3] work, the representation of non-resolved diffusive contributions is achieved deterministically by scaling the resolved diffusive transport terms by a factor to represent the filtered contribution of mass transport from the unresolved transport. For example, if there is no preferred gradient, such as in the presence of a flame brush, a factor of 3 is adopted.

11.3.3.2 Representation of Subfilter-Scale Stresses and Scalar Fluxes

The stochastic contributions represent 3D subfilter-scale advective transport of momentum and scalars (i.e. subfilter-scale stresses and scalar fluxes) resulting from the residual velocity components. For momentum additional contributions may be attributed to pressure scrambling [19]. The stochastic terms are implemented through discrete triplet map events, which are implemented concurrently with other processes within ODT. The rules for stirring events are identical to those applied in stand-alone ODT. The range of length scales for the selected eddies is prescribed prior to the simulation based on a choice of L_{min} and L_{max}, which represent the smallest and largest eddies allowed. The value of L_{min} plays a similar role to the Kolmogorov length scale, and corresponds to length scales where viscous dissipation is predominant and stirring events are less likely to occur. The value of L_{max} determines the cut-off length scale beyond which turbulent advective transport is represented using the filtered advective terms. These parameters are additional model parameters to C and Z prescribed earlier for the ODT-implementation. The cumulative contribution from stirring events over time represents the subfilter-scale stresses and fluxes.

11.3.3.3 Large-Scale Transport

The large-scale transport of momentum and scalars in ODT is represented by the operators $\tilde{u}_j \frac{\partial u_i}{\partial x_j}$, $\tilde{u}_j \frac{\partial T}{\partial x_j}$ and $\tilde{u}_j \frac{\partial Y_k}{\partial x_j}$ in the ODT governing equations. The implementation of large-scale transport represents a fundamental challenge for the following reasons: 1) Advective transport is a 3D process; thus, at least two directions are not resolved on the ODT time scale or on the ODT 1D elements, 2) Non-linear contributions from advection processes pose important constraints on scalar boundedness. In the Cao and Echekki [3] formulation, advective fluxes are constructed at 'nodes' that represent the intersection in space of three or more ODT elements. At these nodes, the solutions of the velocity and scalar equations are updated; then, ODT solutions

between these nodes are updated through single-component advection along the corresponding ODT element. In a Cartesian lattice of ODT elements, these nodes represent the intersection of three orthogonal 1D elements. Below, we describe the implementation based on this Cartesian lattice configuration. The large-scale transport process is implemented as a separate process concurrently with reaction-diffusion and stirring in two steps: 1) node advection, and 2) inter-node relaxation.

Node Advection is implemented as follows. At the prescribed time step for large-scale transport, the solution at each node is evaluated based on gradients represented by the 3 ODT elements intersecting at the node. This process is implemented in two steps. First, the solution is updated at each node for the momentum and scalars using the following governing equations:

$$\frac{\partial \phi^l}{\partial t} = -\tilde{u}_1^1 \frac{\partial \phi^1}{\partial x_1} - \tilde{u}_2^2 \frac{\partial \phi^2}{\partial x_2} - \tilde{u}_3^3 \frac{\partial \phi^3}{\partial x_3} \tag{11.20}$$

In this expression, the dependent variable ϕ corresponds to any one of the variables in the solution vector. The subscripts, 1, 2 or 3, correspond to the components of the velocity vector; while, the superscripts, 1, 2 or 3, correspond to the direction of the ODT domain. Although each node is updated with the same right-hand side that represents contributions from the three directions of ODT elements, its value at the end of the update is different because of the values of ϕ^l are different at the start of the update from the 3 contributing ODT elements. A second step involves the averaging of these 3 solutions at the nodes as follows:

$$\phi^l = \frac{\phi^1 + \phi^2 + \phi^3}{3} \tag{11.21}$$

Inter-Node Relaxation involves a relaxation of the solution between the nodes based on the updated internal boundary conditions at the nodes. This relaxation is accomplished through an integration of the solution at grid cells between the nodes using a single-component advective flux according to the following relation:

$$\frac{\partial \phi^l}{\partial t} = -\kappa \tilde{u}_l^l \frac{\partial \phi^l}{\partial x_l} \tag{11.22}$$

In this expression, κ represents a relaxation coefficient, which governs the rate at which the inter-node solution is updated to reflect changes at the nodes. Because ODTLES is a statistical approach, a range of values for κ may be adopted to yield reasonable statistics for the scalars and momentum solutions.

Similarly to the approach by Schmidt et al. [32], a correction to the ODT velocity solution is implemented such that the filtered ODT velocity field matches the solution from LES.

The above Eulerian formulation was implemented by Cao and Echekki [3] for the modeling of non-homogeneous ignition in a random mixture-fraction field with preheated oxidizer and of the same configurations show that the model represents adequately turbulent transport through the contributions of subfilter-scale transport

and large-scale transport. Important effects of preferential diffusion as well as turbulence intensity are identified in reactive-scalar conditional statistics.

Figure 11.8 shows isocontours of filtered reaction progress variable (normalized temperature) at a prescribed value of 0.5 (for flame tracking) at different times based on the ODTLES simulations. The figure shows the formation of discrete ignition kernels at favorable mixture conditions, their growth and their merger at later times. The reaction progress variable is obtained by filtering the ODT solutions; the size of the initial nascent kernels is smaller than the LES grid.

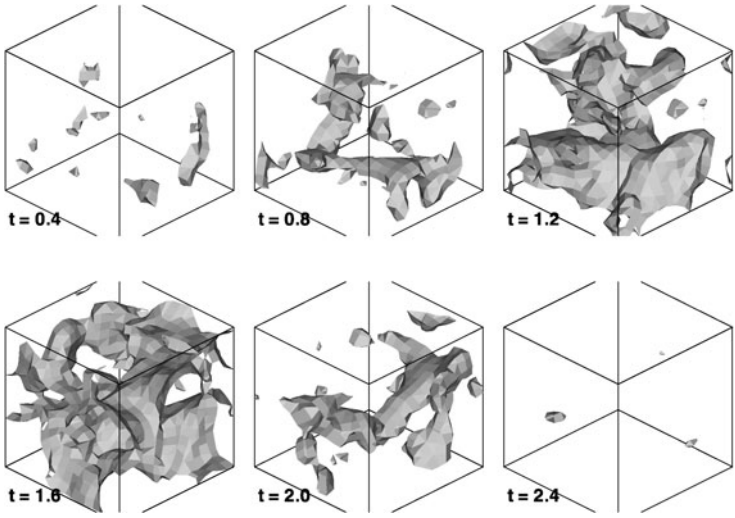

Fig. 11.8: Evolution of flame kernel based on filtered reaction progress variables during non-homogeneous mixture ignition in isotropic turbulence. The figure shows the formation of ignition kernels at conditions favorable to the onset of ignition. Additional kernels are formed at less favorable conditions for autoignition after more delay. The kernels eventually grow to interact at later stages and merge to form larger kernels, until the entire mixture is burned. Reprinted from [3] with permission from Taylor and Francis.

Figure 11.9 shows the evolution of the heat-release rate conditional statistics at two Lewis numbers, 0.5 and 2, representing the ratio of the thermal diffusivity to the species mass diffusivities. The lower Lewis number heat-release rate profiles exhibit higher peaks initially and then lower peaks eventually as the combustion progresses from fuel-lean conditions to richer conditions. The difference between the two cases reflects the strong dependence of the heat release rate on temperature, which is affected by the Lewis number. Lower Lewis numbers indicate slower diffusion of heat relative to species. Therefore, the initial formation of the corresponding kernels favors kernels that shielded from heat loss. However, the same mechanism

may prevent the ignition of the unburned layers next to the ignition kernels and their propagation. Cases a and b shown in comparison with DNS statistics correspond to two different and coarse LES resolutions (case a is twice as resolved as case b). The two cases are in very good agreement with the DNS statistics and show that the ODTLES formulation predicts reasonably well the contributions from large-scale and subfilter-scale transport.

The ODTLES formulation has been extended recently to the study of turbulent premixed flames by Echekki and Park [8]. A Lagrangian formulation has been implemented more recently by Balasubramanian [2] for the study of a buoyant fire plume. In this formulation, the ODT elements are attached to a filtered mixture fraction surface with a fixed value corresponding to the stoichiometric value.

11.4 Concluding Remarks

Here and in Chapter 10, a strategy for turbulent combustion modeling has been outlined that involves a conceptually and computationally minimal representation of the local unsteady evolution of the coupled processes of advection, diffusion, and reaction. ODT, described in this chapter, incorporates a representation of the dependences of the occurrence of eddy motions on the mechanisms that drive these motions. In addition to capturing important effects of the unsteady couplings, this feature results in a formulation that is, in many respects, a self-contained predictive model of turbulent flow. This is perhaps a natural consequence of the effort to capture the couplings relevant to combustion; for a model to do this well, it must capture much of the phenomenology of turbulence.

The main limitation of ODT in this regard is its restriction to one spatial dimension. It is thus complementary to LES, which captures large-scale 3D motions but does not resolve flame structure and evolution. Coupling of ODT to LES has been described. The successes of the LEMLES formulations for the modeling of practical combustion flows (see Chapter 10) also support the potential of ODTLES as a viable modeling approach for similar problems. More importantly, both LEMLES and ODTLES may be viewed as frameworks with which multiphysics and multiphase problems may be addressed. In addition to the momentum and standard scalar equations for combustion problems, additional transport equations may be implemented within these ODTLES frameworks, including particle transport and multiscale descriptions of radiative transport in participating media.

One focus of current efforts is the coupling of arrays of ODT domains so as to obtain a self-contained 3D flow simulation (with the smallest scales resolved only in 1D), thus eliminating the need for a distinct coarse-grained 3D flow solver [17]. This modeling strategy is termed autonomous microstructure evolution (AME). Another focus involves Lagrangian implementation of the ODTLES framework based on ODT elements attached to the flame brush.

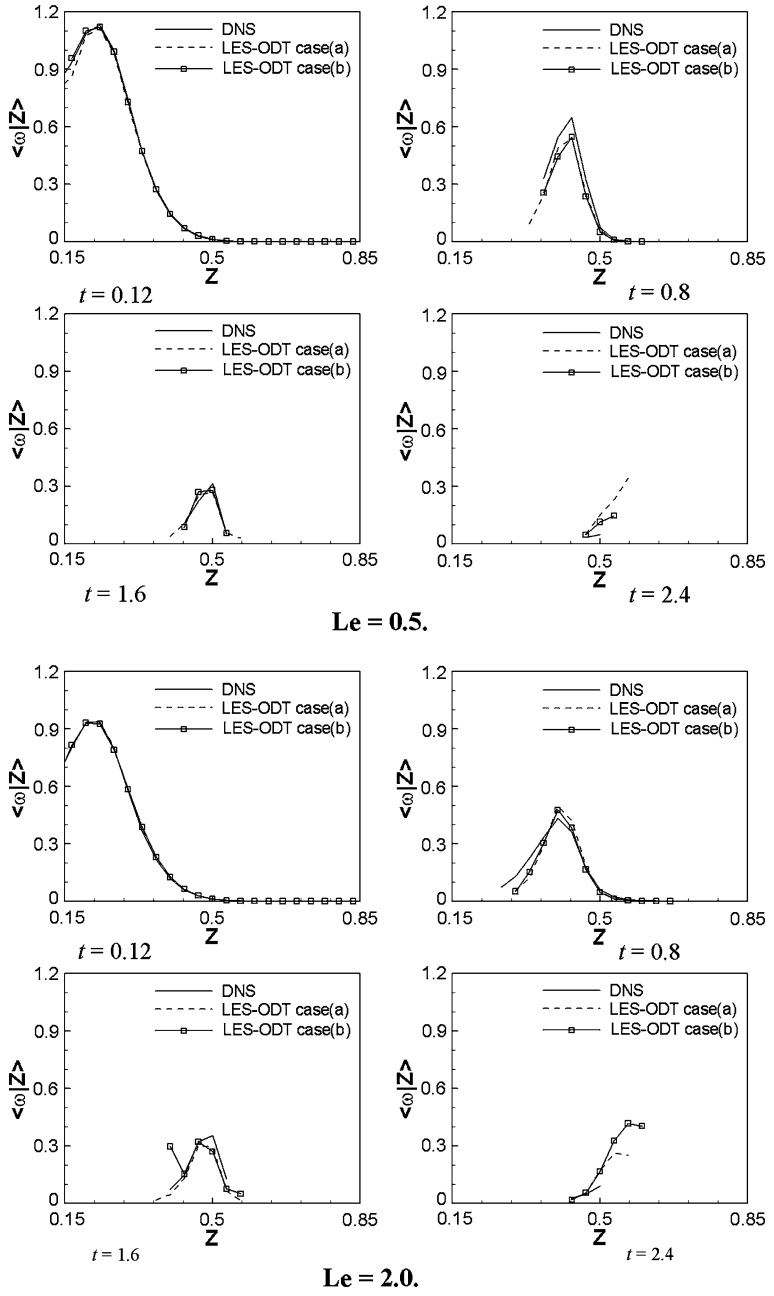

Fig. 11.9: Evolution of the conditional means of the heat release rate conditions during the ignition of a non-homogeneous mixture of fuel and preheat oxidizer at Le = 0.5 and 2.0. Reprinted from [3] with permission from Taylor and Francis.

Acknowledgement

Dr. T. Echekki acknowledges support from the Air Force Office of Scientific Research through grants F49620-03-1-0023 monitored by Dr. Julian Tishkoff and FA9550-09-1-0492 monitored by Dr. Fariba Fahroo and the National Science Foundation through grant DMS-0915150 monitored by Dr. Junping Wang. Dr. A. Kerstein's research was partially supported by the U.S. Department of Energy, Office of Basic Energy Sciences, Division of Chemical Sciences, Geosciences, and Energy Biosciences. Sandia National Laboratories is a multi-program laboratory operated by Sandia Corporation, a Lockheed Martin Company, for the United States Department of Energy under contract DE-AC04-94-AL85000. Dr. J. Sutherland acknowledges support from the Department of Energy under award number FC26-08NT0005015.

References

1. Ashurst, W.T., Kerstein, A.R.: One-dimensional turbulence: Variable-density formulation and application to mixing layers. Phys. Fluids **17**, 025107 (2005)
2. Balasubramanian, S.: A novel approach for the direct simulation of subgrid-scale physics in fire simulations. Master's Thesis, Department of Mechanical and Aerospace Engineering, North Carolina State University (2010)
3. Cao, S., Echekki, T.: A low-dimensional stochatic closure model for combustion large-eddy simulation. J. Turbul. **9**, 1–35 (2008).
4. DesJardin, P.E., O'Hern, T.J., Tieszen, S.R.: Large eddy simulations and experimental measurements of the near field of a large helium-air plume. Phys. Fluids **16**, 1866–1883 (2004)
5. Dreeben, T.D., Kerstein, A.R.: Simulation of vertical slot convection using one-dimensional turbulence. Int. J. Heat Mass Transf. **43**, 3823–3834 (2000)
6. Echekki, T., Gupta, K.: Hydrogen autoignition in a turbulent jet with preheated co-flow air. Int. J. Hydrogen Energy **34**, 8352–8377 (2009)
7. Echekki, T., Kerstein, A.R., Chen, J.-Y., Dreeben, T.D.: One-dimensional turbulence simulation of turbulent jet diffusion flames. Combust. Flame **125**, 1083–1105 (2001)
8. Echekki, T., Park, J.: The LES-ODT model for turbulent premixed flames, AIAA-2010-0207, The 48th AIAA Aerospace Sciences Meeting, Orlando, FL, January 4–7 (2010)
9. http://groups.google.com/group/odt-research
10. Hawkes, E.R., Sankaran, R., Sutherland, J.C., Chen, J.H.: Scalar mixing in direct numerical simulations of temporally-evolving plane jet flames with detailed CO/H_2 kinetics. Proc. Combust. Inst. **31**, 1633–1640 (2007)
11. Hewson, J.C., Kerstein, A.R.: Stochastic simulation of transport and chemical kinetics in turbulent CO/H_2/N_2 flames. Combust. Theory Model. **5**, 559–697 (2001)
12. Hewson, J.C., Kerstein, A.R.: Local extinction and reignition in nonpremixed turbulent CO/H_2/N_2 jet flames. Combust. Sci. Technol. **174**, 35–66 (2002)
13. Kerstein, A.R.: Linear eddy modeling of turbulent transport. 2. Application to shear layer mixing. Combust. Flame **75**, 397–413 (1989)
14. Kerstein, A.R.: Linear-eddy modeling of turbulent transport. 3. Mixing and differential molecular-diffusion in round jets. J. Fluid Mech. **216**, 411–435 (1990)
15. Kerstein, A.R.: One-dimensional turbulence: Model formulation and application to homogeneous turbulence, shear flows, and buoyant stratified flows. J. Fluid Mech. **392**, 277–334 (1999)

16. Kerstein, A.R.: One-dimensional turbulence. Part 2. Staircases in double-diffusive convection. Dyn. Atmos. Oceans **30**, 25–46 (1999)
17. Kerstein, A.R.: Lect. Notes Phys. **756**, 291–333 (2009)
18. Kerstein, A.R.: One-dimensional turbulence: A new approach to high-fidelity subgrid closure of turbulent flow simulations. Computer Phys. Commun. **148**, 1–16 (2002)
19. Kerstein, A.R., Ashurst, Wm.T., Wunsch, S., Nilsen, V.: One-dimensional turbulence: Vector formulation and application to free shear flows. J. Fluid Mech. **447**, 85–109 (2001)
20. Kerstein, A.R., Wunsch, S.: Simulation of a stably stratified atmospheric boundary layer using one-dimensional turbulence. Bound. Layer Meteorol. **118**, 325–356 (2006)
21. Krishnamoorthy, N.: Reaction models and reaction state parameterization for turbulent non-premixed combustion. Ph.D. Thesis, University of Utah, Salt Lake City (2008)
22. Law, A.M., Kelton, W.D.: *Simulation Modeling and Analysis*, 3rd Ed. (McGraw-Hill, New York 2000)
23. McDermott, R.J.: Toward one-dimensional turbulence subgrid closure for large-eddy simulation. Ph.D. Thesis, University of Utah, Salt Lake City (2005)
24. McDermott, R.J., Kerstein, A.R., Schmidt, R.C., Smith, P.J.: The ensemble mean limit of the one-dimensional turbulence model and application to finite-volume large-eddy simulation. J. Turbul. **6**, 1–33 (2005)
25. Peters, N., *Turbulent Combustion* (Cambridge Univ. Press, Cambridge 2000)
26. Punati, N., Sutherland, J.C.: Application of an Eulerian one dimensional turbulence model to simulation of turbulent jets, U.S. Joint Sections of the Combustion Institute, Ann Arbor, MI, May (2009)
27. Punati, N., Sutherland, J.C., Kerstein, A.R., Hawkes, E.R., Chen, J.H.: An evaluation of the one-dimensional turbulence model: Comparison with direct numerical simulations of CO/H_2 jets with extinction and reignition. Proc. Combust. Instit., to appear (2011)
28. Ranganath, B., Echekki, T.: One-dimensional turbulence-based closure for turbulent non-premixed flames. Prog. Comput. Fluid Dyn. **6**, 409–418 (2006)
29. Ranganath, B., Echekki, T.: One-dimensional turbulence-based closure with extinction and reignition. Combust. Flame **154**, 23–46 (2008)
30. Ranganath, B., Echekki, T.: ODT closure with extinction and reignition in piloted methane-air jet diffusion flame. Combust. Sci. Technol. **181**, 570–596 (2009)
31. Ricks, A.J., Hewson, J.C., Kerstein, A.R., Gore, J.P., Tieszen, S.R., Ashurst, Wm.T.: A spatially-developing one-dimensional turbulence (ODT) study of soot and enthalpy evolution in meter-scale buoyant turbulent flames. Combust. Sci. Technol. **182**, 60–101 (2010)
32. Schmidt, R.C., Kerstein, A.R., McDermott, R.: ODTLES: A multi-scale model for 3D turbulent flow based on one-dimensional turbulence modeling. Comput. Methods. Appl. Mech. Engg. **199**, 865–880 (2010)
33. Schmidt, R.C., Kerstein, A.R., Wunsch, S., Nilsen, V.: Near-wall LES closure based on one-dimensional turbulence modeling. J. Comput. Phys. **186**, 317–355 (2003)
34. Schmidt, J.R., Wendt, J.O.L., Kerstein, A.R.: Non-equilibrium wall deposition of inertial particles in turbulent flow. J. Stat. Phys. **137**, 233–257 (2009)
35. Shihn, H., DesJardin, P.E.: Simulation of vertical wall fires with one-dimensional turbulence modeling. Spring Technical Meeting, The Combustion Institute/Canadian Section, Ontario, Canada, May 9–12 (2004)
36. Shihn, H., Desjardin, P.E.: Near-wall modeling of an isothermal vertical wall using one-dimensional turbulence. Int. J. Heat Mass Transf. **50**, 1314–1327 (2007).
37. Sutherland, J.C., Punati, N., Kerstein, A.R.: A unified approach to the various formulations of the one-dimensional turbulence model. Technical Report ICSE100101, The University of Utah Institute for Clean and Secure Energy, Salt Lake City, UT, 2010. Available from (accessed June 2010): http://repository.icse.utah.edu/dspace/handle/123456789/9861
38. Wunsch, S.: Stochastic simulations of buoyancy-reversal experiments. Phys. Fluids **15**, 1442–1456 (2003)

39. Wunsch, S., Kerstein, A.R.: A model for layer formation in stably-stratified turbulence. Phys. Fluids **13**, 702–712 (2001)
40. Wunsch, S., Kerstein, A.R.: A stochastic model for high Rayleigh-number convection. J. Fluid Mech. **528**, 173–205 (2005)